Science of the Total Environment 505 (2015) 102–112

Contents lists available at ScienceDirect

Science of the Total Environment

journal homepage: www.elsevier.com/locate/scitotenv

Evaluation of slow pyrolyzed wood and rice husks biochar for adsorption of ammonium nitrogen from piggery manure anaerobic digestate slurry

Simon Kizito [a], Shubiao Wu [a,*], W. Kipkemoi Kirui [a], Ming Lei [b], Qimin Lu [a], Hamidou Bah [a], Renjie Dong [a]

[a] Key Laboratory of Clean Utilization Technology for Renewable Energy in Ministry of Agriculture, College of Engineering, China Agricultural University, 100083 Beijing, PR China
[b] College of Agronomy and Biotechnology, China Agricultural University, 100083 Beijing, PR China

HIGHLIGHTS

- Biochar adsorbed 60% NH_4^+-N from piggery slurry.
- Absorption was sensitive to changes in particle size, pH and temperature.
- NH_4^+-N adsorption from slurry followed the Langmuir and Pseudo second order models.
- Monolayer chemisorption was the major NH_4^+-N adsorption mechanism from piggery slurry.

ARTICLE INFO

Article history:
Received 4 July 2014
Received in revised form 25 September 2014
Accepted 28 September 2014
Available online 10 October 2014

Editor: Simon Pollard

Keywords:
Biochar
Piggery manure anaerobic digestate
Ammonium adsorption
Kinetics
Thermodynamics

ABSTRACT

Due to its high adsorption capacity, the use of biochar to capture excess nutrients from wastewater has become a central focus in environmental remediation studies. In this study, its potential use in adsorption and removal of ammonium in piggery manure anaerobic digestate slurry was investigated. The adsorbed amount of NH_4^+-N ($mg \cdot g^{-1}$) and removal percentage as a function of adsorbent mass in solution, adsorbent particle size, NH_4^+-N concentration in the effluent, contact time, pH and temperature were quantified in batch equilibrium and kinetics experiments. The maximum NH_4^+-N adsorption from slurry at 1400 mg $N \cdot L^{-1}$ was 44.64 ± 0.602 $mg \cdot g^{-1}$ and 39.8 ± 0.54 $mg \cdot g^{-1}$ for wood and rice husk biochar, respectively. For both biochars, adsorption increased with increase in contact time, temperature, pH and NH_4^+-N concentration but it decreased with increase in biochar particle size. Furthermore, the sorption process was endothermic and followed Langmuir ($R^2 = 0.995$ and 0.998) and Pseudo-second order kinetic models ($R^2 = 0.998$ and 0.999). Based on the removal amounts, we concluded that rice husk and wood biochar have potential to adsorb NH_4^+-N from piggery manure anaerobic digestate slurry, and thus can be used as nutrient filters prior to discharge into water streams.

1. Introduction

Over the years the promotion of scaled piggery farms in China has greatly helped in closing the gap between products supply and demand. However, the huge amounts of manure and related wastes produced are causing an unforeseen environmental pollution (Huaitalla et al., 2013). Piggery farms generate solid manure (feces), raw manure slurry (urine and wash water), and digestate slurry after biodigester treatment. These three waste streams are renowned for containing high nutrients mainly nitrogen and phosphorus compounds but also contain high Chemical and Biological Oxygen Demanding organics (COD and BOD) that often pollute the environment (FAO, 2006). In the past decade, manure nutrients could be efficiently recycled back to because of the high integration of livestock production with cropping cycles (Chen, 1997). To date, the threshold for piggery production has shifted from small scale rural farming communities to large scaled production in the suburbs of major cities. Consequently, the manure nutrients and wastewater produced by the peri-urban farms are far more than can be recycled as fertilizer on nearby land (Chen et al., 2012). The agricultural recycling loop has been ruptured by the extra cost of transporting large volumes of nutrients slurry from urban farms to rural crop farming areas. Furthermore, the rapid development in rural China has increased land fragmentation and as a result, the rural farming methods have gradually changed with now more farmers preferring the use of mineral fertilizers over manure for intensive production on small cropping areas. This shift in farming methods has greatly reduced the potential of agricultural assimilation of large scale nutrients and implying the need for other alternatives to land disposal that could reduce environmental pollution risks.

In China at present the entire livestock industry still lacks adequate manure treatment facilities and pollution is further driven by the weak pollution reinforcement (Gale et al., 2012; Yang et al., 2012). Traditionally, it is common to store the daily generated manure slurry

* Corresponding author. Tel.: +86 10 62737852; fax: +86 10 62737885.
E-mail address: wushubiao@gmail.com (S. Wu).

http://dx.doi.org/10.1016/j.scitotenv.2014.09.096
0048-9697/

in large open lagoons for while to allow for aerobic degradation and after the effluents with their residual nutrients are discharged into the environment. Besides lagoons, anaerobic digestion (AD) with biogas supply is gradually gaining ground as a large scale manure treatment procedure (Chen et al., 2012). The production of biogas has an added advantage of lowering farm energy costs through utilization of the gas directly or for electricity generation. However, considering that during anaerobic digestion limited nitrification occurs, the digestate remains rich in NH_4^+-N in addition to the residual COD, BOD and phosphorous compounds and therefore the disposal challenge of residual slurry remains unsolved. Often times depending on animal stocking density and the digester capacities, the cost of slurry handling and transportation becomes economically unfeasible and farms tend to discharge their waste without any secondary pretreatment to nearby water streams causing heavy pollution.

According to the China pollution source census carried out in 2010, the COD, total nitrogen (TN) and phosphorus from the livestock breeding industry accounted for 96%, 38% and 56% of the total pollutants from agricultural sources respectively and were 2.3 times that of industrial sources. By no surprise, the highest values for this form of pollution were reported in commercial piggery farming areas in Sichuan, Shandong, Guangdong, Henan and Zhejiang provinces (China Ministry of Environmental Protection, 2010). In these provinces, massive eutrophication has caused heavy algae blooms killing fish and other aquatic life. Human life has also been endangered through reduced amount of usable water and reduced aquatic food supply (Nielsen et al., 2013). Therefore, in order to balance livestock production with human welfare and the environment it is imperative to control pollution from manure nutrients and definitely as earlier discussed agricultural recycling and anaerobic digestion alone without recovery of nutrients in the residual slurry is no longer a solution.

In literature, several methods ranging from biological, physical, chemical or a combination of these have been explored to manage pollution from livestock sources. The chemical approach has focused on the use of struvite to recover N and P from livestock liquid manure (Ganrot et al., 2007; Nelson et al., 2003; Song et al., 2011; Turker and Celen, 2007; Wrigley et al., 1992) Biologically, ammonium removal using membrane reactors, anaerobic ammonium oxidation (ANAMMOX), sequential combined aerobic and anaerobic batch reactors (SBR) and denitrification in constructed wetlands have received reasonable research attention (Değermenci et al., 2012; Harrington and Scholz, 2010; Healy et al., 2007; Molle et al., 2008). Likewise, adsorption methods with activated carbons, ion exchange resins and zeolites for ammonia removal have been widely explored (Huang et al., 2010; Nguyen and Tanner, 1997; Sica et al., 2014; Thornton et al., 2007). Despite the reported success, the challenge with all the above mentioned methods still remains the high cost of raw materials and the initial process set up especially for large scale projects (Song et al., 2011). In addition, full scale application of biological processes for ammonium removal is technically limited by the high microbial sensitivity to shock loadings and pH changes in the waste water which require pH correction while the more nitrate generated necessitates further removal (Sica et al., 2014).

In the present study, the potential use of biochar is proposed as an alternative treatment for NH_4^+-N removal from piggery manure anaerobic digestate slurry. Biochar is described as porous solid carbonaceous material producible through pyrolysis of a wide range of biomass in anoxic conditions at temperatures ranges of 300–1500 °C (Ahmedna et al., 1997b). Due to its favorable characteristics such as high surface area, high porosity, cation exchange capacity and pH buffering ability, biochar has received overwhelming attention in agronomic studies for soil amendment and carbon sequestration (Mukherjee et al., 2014; Mukherjee and Zimmerman, 2013; Novak et al., 2010; Rajkovich et al., 2011; Spokas et al., 2011; Taghizadeh-Toosi et al., 2012b). Biochar has also emerged as a potential biomaterial for adsorption of nutrients and different organic pollutants from domestic, agricultural and industrial waste waters (Amuda et al., 2007; Chen et al., 2011; Kim et al., 2013; Mizuta et al., 2004; Sarkhot et al., 2013; Zheng et al., 2010; Zhu et al., 2012). However, from our literature survey, the application of biochar to treat piggery manure anaerobic digestate slurry for nutrient recovery and water recycling has not been fully researched. This study therefore focuses on (a) understanding the effects of biochar dosage, particle size, pH, effluent concentration, temperature and adsorption time on the NH_4^+-N removal efficiency from the slurry and (b) evaluating the process kinetics and thermodynamics of NH_4^+-N adsorption onto biochar derived from wood residues and rice husks. This work is part of a larger research project aimed at developing on-farm livestock wastewater treatment technologies based on biochar adsorption to recycle nutrients and re-use water. Therefore, the preliminary results on adsorption dependent factors and kinetics will provide empirical information useful for the design of future adsorption facilities on a pilot scale.

2. Materials and methods

2.1. Biochar characterization

The biochar was produced from mixed wood cuttings and rice husks under slow pyrolysis at 600 °C for a retention time of 10 h. Proximate analysis was done to measure moisture content, fixed carbon, volatiles and ash content according to ASTM D-1762-84 standard for analysis of charcoal (ASTM, 2007). In brief, the moisture content was determined on dry matter basis after drying the samples in open crucibles at 105 °C for 24 h. The ash content was determined by combustion of biochar samples in an open ceramic crucible at 700 °C for 6 h. Volatile matter content was determined as weight loss after combustion in a ceramic crucible with a loose ceramic cap at 950 °C for 10 min while the fixed carbon was calculated by difference. The elemental composition of carbon, hydrogen, nitrogen, oxygen and sulfur of biochar samples was done based on the dry combustion method using a CHNS/O Elemental Analyzer (Vario MACRO, Germany). The biochar bulk density, pH and electro-conductivity were determined with slight modification of the method described by Ahmedna et al. (1997). Briefly, five tubes of 10 ml volume capacity were filled with dry ground biochar and gently tamped to a constant volume. The bulk density was then calculated by dividing the weight of each tube by the volume of the packed biochar material. To measure the pH and electro-conductivity, suspensions of biochar were prepared by diluting 1 g biochar with 20 ml de-ionized (Milli-Q pore) water. The suspensions (in triplicate) were then shaken at 90 °C in an end to end shaker for 2 h to allow the dissolution of the soluble biochar components, after which the pH was measured with a pH-meter (Metler Toledo) and the electro-conductivity was read using a EC meter (Orion Model 115A, Thermal Fisher Scientific, USA). Brunauer–Emmett–Teller method with N_2 adsorption at 77 K was used to investigate the surface area and porosity of the biochar. Scanning electron microscopy technique was used to study the morphology of the adsorbent while surface and structural chemical functional groups in the biochar were studied using the Fourier Transform Infrared technique (FT-IR, Spectrum 100, Perkin Elmer) with an intensity of 4000–400 cm^{-1} (Fu et al., 2012). Table 1 gives a summary of the measured parameters.

2.2. Sampling and slurry characterization

Pretreated slurry samples were collected from a mesophilic biogas plant digesting solely piggery manure with an anaerobic digestate slurry capacity of 10 m^3 day^{-1}. The plant is located in Dong Hua Shan Village, Beijing. The collection time was from November 2013 to February 2014. Prior to use, the slurry was centrifuged at 12,000 rpm for 15 min and the supernatant was filtered through a 0.45 μm cellulose acetate membrane to remove residual colloidal matter. One part of the filtrate was used in determination of the organic and inorganic parameters while the other part was stored at 3 ± 1 °C prior to sorption

Table 1
Biochar characteristics.

Parameter	Unit	Wood biochar	Rice husk biochar
BET surface area	($m^2 \cdot g^{-1}$)	273.623	10.995
Total pore volume	($ml \cdot g^{-1}$)	0.176	0.038
Micro pore volume	($ml \cdot g^{-1}$)	0.1123	0.0044
Bulk density	($g.\ ml^{-1}$)	0.4994	0.2980
EC	($\mu s\ cm^{-1}$)	411.0	299.8
pH	–	9.80	7.80
MC	(%)	5.06	5.33
Ash	(%)	5.87	41.96
Volatile content	(%)	8.92	35.67
Fixed carbon	(%)	80.2	17.34
Elemental composition			
Carbon [a]	(%)	86.3	37.91
Hydrogen [a]	(%)	0.79	2.06
Nitrogen [a]	(%)	0.73	0.89
Sulfur	(%)	0.22	2.06
Oxygen [b]	(%)	12.18	59.14
H/C [c]	–	0.0092	0.054
O/C [c]	–	0.141	1.560

[a] Estimated on an ash free basis.
[b] Estimated as difference.
[c] Estimated on a mass/mass basis.

experiments. The American Public Health Association Standard methods (APHA, 2005) were used in the determination of biological oxygen demand and soluble chemical oxygen demand, nitrogen compounds (NH_4^+-N, NO_3^--N, NO_2^--N) and PO_4^{3-}-P in the filtrate samples. Total organic carbon in the filtrated slurry sample was determined by TOC Analyzer (Model TOC-VPN, Shimadzu, Japan). For heavy metal analysis different methods were employed depending on the target ion. Inductive Coupled Plasma Mass Spectrometry (ICP-MS-*X2*, Thermal Fisher., USA) was used to analyze ions of Zn, Cu, Sr, Ni, Al, Co, As, Mn, Ba, Cr, Se, Pb and Cd. Atomic Adsorption Spectrophotometer (TAS-990; Purkinje General, China) was used to analyze Fe, K and Na ions whereas Ca and Mg were analyzed using EDTA titration method (GB/T7476-1987). The pH was measured directly in both the non-centrifuged and centrifuged samples using a digital pH meter (FE20, METTLER TOLEDO, Switzerland). The measured parameters are summarized in Table 2.

Table 2
Summary of anaerobic digestate slurry characteristics.

Biological parameter	Symbol	Unit	Estimated value
pH	–		8.0–8.3
Electro conductivity	(EC)	($\mu s.\ cm{-}^3$)	104
Soluble chemical oxygen demand	SCOD	($mg \cdot L^{-1}$)	4500–5000
Biological oxygen demand	BOD_5	($mg \cdot L^{-1}$)	430–510
Total solid	TS	($mg \cdot L^{-1}$)	15–18
Ammoniac nitrogen	NH_4-N	($mg \cdot L^{-1}$)	1390–1450
Nitrate nitrogen	NO_3-N	($mg \cdot L^{-1}$)	47–54
Nitrite nitrogen	NO_2-N	($mg \cdot L^{-1}$)	34–56
Ortho-phosphate	PO_4-P	($mg \cdot L^{-1}$)	15–20
Total organic carbon	TOC	($mg \cdot L^{-1}$)	226.1 ± 10.9
*Metal ions**			
Potassium	K	($mg \cdot L^{-1}$)	1205.75 ± 9.81
Sodium	Na	($mg \cdot L^{-1}$)	301.5 ± 1.00
Calcium	Ca	($mg \cdot L^{-1}$)	48.7 ± 5.459
Magnesium	Mg	($mg \cdot L^{-1}$)	39.45 ± 4.729
Ferrous Iron	Fe	($mg \cdot L^{-1}$)	3.74 ± 0.694
Zinc	Zn	($mg \cdot L^{-1}$)	0.583 ± 0.250
Copper	Cu	($mg \cdot L^{-1}$)	0.296 ± 0.139
Strontium	Sr	($mg \cdot L^{-1}$)	0.184 ± 0.005

* Sr, Ni, Al, Co, As, Mn, Ba, Cr, Se, Pb, Cd are not reported because their concentrations were < 0.1 ($mg \cdot L^{-1}$).

2.3. Experimental setup for batch adsorption

Adsorption was studied in pure NH_4Cl solution and piggery slurry. The adsorption arising from the pure solution was used as a benchmark to investigate differences in the adsorption phenomena in manure slurry (Sarkhot et al., 2013). The slurry was diluted to make NH_4^+-N concentrations of 250, 500, 750, 1000 and 1400 $mg \cdot N \cdot L^{-1}$. The NH_4Cl stock solution was prepared from a 99.5% pure anhydrous solid by dissolution in distilled water. From this stock solution, dilutions with distilled water were made to achieve similar concentrations as for the slurry. To determine the most appropriate pH, maximum adsorption time and most efficient dosage of the adsorbent, preliminary experiments were done at room temperature (25 °C) with biochar dosages of 0.1 to 5 g, particle size of 0.25 mm, at pH of 3 to 9. Briefly, 0.1 to 5 g biochar was transferred into 100 ml transparent plastic bottles. To the bottles, 50 ml of 1000 $mg \cdot L^{-1}$ NH_4Cl and slurry solution was added and the pH adjusted using 0.1 N NaOH/HCl solutions and the bottles tightly sealed. Duplicate control samples containing only nutrient solutions were set up to examine ammonium reduction from other sources other than biochar adsorption. All the bottles including controls were transferred into a water bath shaker to equilibrate for 96 h at an agitation speed of 120 rpm. At the end of 96 h, the bottle contents (with exception of the controls) were centrifuged at 7500 rpm for 15 min to separate the solid and liquid phases. After separation, 10 ml of the supernatant were filtered through a 0.45 μm cellulose acetate membrane and from the filtrate the residual amount of NH_4^+ in solution was determined colorimetrically using UV spectrophotometer (Shimadzu UV-1800, Japan) by monitoring the absorbance changes at 697 nm.

The removal percentage and equilibrium amount of NH_4^+-N adsorbed per unit mass of adsorbent were calculated using the following equations:

$$\%\ \text{Removal} = \frac{[C_o - C_e]}{C_o} * 100 \quad (1)$$

$$Q_e = \frac{[C_o - C_e] * V}{W_b} \quad (2)$$

where; C_o and C_e ($mg \cdot L^{-1}$) are the initial and equilibrium NH_4^+-N concentrations in solution respectively, Q_e ($mg \cdot g^{-1}$) was the adsorbed amount of NH_4^+-N at equilibrium, V (L) was the volume of solution used, and W_b (g) the mass of biochar.

From preliminary results NH_4^+ reduction from the controls was minimal i.e., 0.4–1% from NH_4Cl solution and 0.8–1.5% from slurry. Based on this result it was assumed for the rest of tests that the biggest part of ammonium was adsorbed onto the biochar. From the biochar–nutrient mixture samples, it was observed that at pH between 6.5 and 7.0, both rice husk and wood biochar at a dosage of 1 to 1.5 g could remove up to 80% of the total NH_4^+ ions adsorbed from the solution and beyond 2 g there was no reasonable addition in amounts adsorbed. This maximum adsorption was also observed to occur after 20 h of shaking beyond which marginal adsorption decreased. Therefore, subsequent batch adsorption studies were investigated at pH = 7, using 1 g of biochar with 50 mL of the effluent (NH_4Cl and slurry). More so, the influence of increasing biochar particle sizes (0.25–1.25 mm), effluent NH_4^+-N concentration (250–1400 $mg \cdot L^{-1}$) and temperature (288–318 K) on NH_4^+-N adsorption were investigated.

2.4. Modeling the adsorption data

From literature, adsorption isotherms are handy in describing how pollutants interact with adsorbent materials and so they are critical to optimizing the use of adsorbents. On the other hand, the study of adsorption kinetics has been widely employed to understand the mechanisms that are involved and the dynamics of NH_4^+ adsorption (Hale

et al., 2013; Long et al., 2008; Zhu et al., 2012). In this study in order to evaluate the kinetics and thermodynamic phenomena of NH_4^+ adsorption onto the biochar, the NH_4^+-N adsorbed at equilibrium (Q_e, mg·g^{-1}) and residual equilibrium NH_4^+-N concentration in solution (C_e, mg·L^{-1}) at different initial ammonium concentrations, contact time and temperature were fitted to the; Langmuir, Freundlich, Pseudo-first order and Pseudo-second order kinetic models, the Intrapartical model and the van't Hoff's equation.

2.4.1. Adsorption isotherms

The Langmuir equation is given by;

$$\frac{C_e}{Q_e} = \frac{1}{\alpha\beta} + \frac{\alpha}{C_e}. \quad (3)$$

The Freundlich equation is given by;

$$\text{Log } Q_e = \text{Log } K_f + \frac{1}{n}\text{Log } C_e \quad (4)$$

where;Q_e (mg·g^{-1}) is the adsorbed amount per unit mass of biochar, 'α' (mg·g^{-1}) and 'β' (L.mg^{-1}) are Langmuir constants that indicate the maximum adsorption and relative binding energy of the biochar, respectively. K_f and 'n' are Freundlich constants that measure the relative NH_4^+ adsorption capacity and adsorption intensity of the biochar respectively; while C_e (mg·L^{-1}) denotes the equilibrium concentration of NH_4^+ remaining in solution after adsorption is complete.

For the Langmuir model, plotting (C_e/Q_e) against C_e both 'α' and 'β' were determined as the slope ($1/\alpha$) and intercept ($1/\alpha\beta$), respectively. Conversely, for the Freundlich model, the constants 'K_f' and 'n' were determined from the plot of Log Q_e against Log C_e as the intercept (Log K_f) and slope ($1/n$). The graphical plots for both models are depicted in Fig. 4 while the statistical calculation for rate constants is presented in Table 4.

2.4.2. Adsorption kinetics

Similar to batch tests, kinetic experiments were done using 1 g biochar in 50 ml wastewater. The ammonium sorption was investigated at three initial concentrations i.e., 500, 1000 and 1400 mg·L^{-1} at a temperature of 308 K and contact time ranging from 60 min to 1440 min. At predetermined time intervals the samples were taken out and the residual NH_4^+ concentrations were determined spectrophotometrically while the removal percentage and adsorbed amount (mg·g^{-1}) were calculated using Eqs. (1) and (2). Eventually, adsorption data at different contact times was fitted to the intrapartical model and to the pseudo-first order and pseudo-second order models.

For the pseudo first and second order models, the following expressions were used (Ho and McKay, 1999)

$$\text{Log } (Q_1 - Q_t) = \text{Log } (Q_1) - \frac{\lambda_1}{2.0303}t \quad \text{[First order]} \quad (5)$$

$$\frac{t}{Q_t} = \frac{1}{\lambda_2 Q^2{}_2} + \frac{1}{Q_2}t \quad \text{[Second order]} \quad (6)$$

where,Q_1, and Q_2 (mg·g^{-1}) are the adsorbed amounts of NH_4^+-N at equilibrium.

Q_t was the adsorbed amount at a given time interval (t) while λ_1 and λ_2 (min^{-1}) are the rate constants calculated from the straight-line plot of log (Q_1–Q_t) against time (t) and t/Q_t against t, for the pseudo-first and second order models, respectively. The graphical plots of the models and the computed rate constants are presented in Fig. 5(a) and (b), and Table 5.

The following expression was used for the intrapartical model (Qu et al., 2008).

$$q_t = K_d t^{1/2} + C \quad (7)$$

where;K_d is the intrapartical diffusion rate constant (mg·g^{-1} min$^{1/2}$), C (mg·g^{-1}) is a constant that reflects the boundary layer effect. A plot of q_t against $t^{1/2}$ gave a linear relationship from which the K_d value was determined from the slope and C as the intercept. The graphical plots of the model and the computed rate constants are presented in Fig. 5c and Table 5.

2.4.3. Adsorption thermodynamics

In order to understand the thermodynamic phenomena of NH_4^+ adsorption onto the biochar, sorption data using initial NH_4^+-N concentration of 1000 mg·L^{-1} at a temperature range of 15–45 °C were collected after 24 h equilibration time. From the equilibrium data four parameters; free energy change ($\Delta G°$), enthalpy change ($\Delta H°$), entropy change ($\Delta S°$) and thermodynamics constant (K_c) were calculated to confirm the nature of the adsorption process (Kucic et al., 2013; Nidheesh et al., 2012). The thermodynamic equilibrium constant K_c, was defined as;

$$K_c = \frac{C_o - C_e}{C_e} \quad (8)$$

where;C_o and C_e (mg·L^{-1}) are the initial and equilibrium concentration of ammonium solution.

The Gibb's free energy change ($\Delta G°$), of the process was related to the K_c by the following equation;

$$\Delta G^o = -RT \ln K_c \quad (9)$$

where;T is temperature in K, R the ideal gas constant = 8.314 J mol^{-1} K^{-1}

Table 3
Equilibrium adsorption amount (Q_e, mg·g^{-1}) and NH_4^+-N removal efficiency (% R_{ef}) of biochar at varying initial concentrations in anaerobic digestate slurry and pure NH_4Cl solution at 35 °C, pH = 7.

	Wood biochar			
	NH_4Cl solution		Slurry	
Co (mg·L^{-1})	Q_e (mg·g^{-1})	R_{ef} (%)	Q_e (mg·g^{-1})	R_{ef} (%)
250	11.35	90.81	9.73	77.85
500	21.66	86.63	18.32	73.28
750	31.51	84.03	26.28	70.07
1000	40.78	81.55	33.30	66.60
1400	54.86	73.14	42.02	60.03
Co (mg·L^{-1})	**Rice husk biochar NH_4Cl solution Q_e (mg·g^{-1})**	**R_{ef} (%)**	**Slurry Q_e (mg·g^{-1})**	**R_{ef} (%)**
250	10.51	84.08	9.14	73.14
500	20.34	81.36	17.18	68.71
750	29.41	78.44	25.08	66.88
1000	37.11	74.22	30.99	61.99
1400	47.14	62.85	37.63	53.76

Table 4
Model fit data for Langmuir and Freundlich isotherms explaining NH_4^+-N from NH_4Cl and anaerobic digestate slurry solutions by biochar.

	Langmuir model			Freundlich model		
Biochar	α (mg·g^{-1})	β (L·mg^{-1}) × 10^{-3}	R_L^2	K_F (mg·g^{-1})	1/n	R_F^2
WDB_1	133.33	5.840	0.998	0.6132	1.422	0.993
WDB_2	78.06	2.496	0.995	0.6644	1.522	0.987
RHB_1	71.94	5.895	0.994	0.6604	1.487	0.985
RHB_2	59.56	2.739	0.993	0.1675	1.564	0.977

The subscripts 1 and 2 on wood (WDB) and rice (RHB) biochar denote adsorption from pure NH_4Cl and slurry solutions respectively.

Table 5
Model fit data for the kinetic equations using pure NH_4Cl and anaerobic digestate slurry solution.

Biochar	Pseudo first order				Pseudo second order				Intrapartical		
	q_e ($mg \cdot g^{-1}$)	Q_1 ($mg \cdot g^{-1}$)	$\lambda_1 \times 10^{-3}$	R^2	Q_2 ($mg \cdot g^{-1}$)	$\lambda_2 \times 10^{-3}$	$V = (\lambda_2 Q^2_2)$ ($mg \cdot g^{-1}\ min^{-1}$)	R^2	K_d ($mg \cdot g^{-1}\ min^{-1}$)	C ($mg \cdot g^{-1}$)	R^2
WDB_1	42.30	37.24	3.16	0.920	28.43	1.064	0.860	0.998	1.147	15.13	0.963
WDB_2	33.05	18.20	2.54	0.842	30.03	1.113	1.004	0.988	1.860	15.40	0.945
RHB_1	38.31	33.88	4.60	0.971	41.98	1.345	2.370	0.999	1.203	13.40	0.897
RHB_2	30.76	13.80	2.56	0.857	46.21	1.151	2.458	0.995	1.857	14.05	0.924

The subscripts 1 and 2 on wood biochar (WD) and rice biochar (RHB) denote adsorption from pure NH_4Cl and slurry solutions respectively at initial concentration of 1000 mgL^{-1}.

Conversely, according to van't Hoff's thermodynamics equation, the Gibb's free energy was related to the enthalpy change ($\Delta H°$) and entropy change ($\Delta S°$) at constant temperature by the following expression.

$$\text{In } K_c = -\frac{\Delta G^o}{RT} = -\frac{\Delta H^o}{RT} + \frac{\Delta S^o}{R} \quad (10)$$

Thus, from the linear plot of ln *Kc* versus 1/T, the enthalpy ($\Delta H°$) and entropy ($\Delta S°$) values were calculated from the slope ($^{\Delta S}/_{R}$) and intercept ($^{\Delta H}/_{RT}$), respectively. The graphical plots of the model are depicted in Fig. 3b and the statistical parameters are presented in Table 6.

2.5. Statistical analysis of data

The adsorption and kinetics data were collected in triplicates. Descriptive statistics was used to obtain means, standard deviation and standard errors. Regression analysis was used to fit sorption, kinetic and thermodynamic isotherms. The Chi-square data fit function (χ^2) and adjusted regression (R^2) coefficients were used to verify model fits. One way ANOVA was used to predict significant differences in NH_4^+ adsorption by biochar from the two nutrient solutions. In cases where differences occurred, the Fisher Multiple Comparison of means was performed. All inferential analysis was done at 95% ($p \leq 0.05$) confidence level using *Sigma Plot* version 12.5.

3. Results and discussion

3.1. Biochar properties

The biochar characteristics are presented in Table 1. From the table, surface area of wood derived biochar was much higher than that of rice husk biochar. Similarly, the fixed carbon content, electro-conductivity and pH of wood biochar were higher compared to that of rice husks biochar. The rice husk biochar however, had higher ash, volatile, sulfur and nitrogen contents. According to previous studies, the discrepancies in ash, volatile and fixed carbon contents can be linked to the chemical composition differences between wood and rice husks. Wood contains more cellulose and hemicelluloses and during high temperature pyrolysis (>500 °C), the components are reduced to carbon thus the higher fixed carbon content in wood biochar (Ahamedna et al., 2000; Al-Wabel et al., 2013; Keiluweit et al., 2010). On the other hand, rice husks contain high amounts of silicon and mineral elements concentration thus the high ash content (Abdulrazzaq et al., 2014). The scanning electron microscopy images (Fig. 1) for both the biochars showed wood biochar had a more crystalline structure with multiple voids and micropores. Conversely, the rice husk biochar images showed a more amorphous and less porous structure. According to Keiluweit et al. (2010), crystalline structures result from dehydration of cellulose and thus compared to wood, rice husks have lower content of cellulose and this explains the more amorphous structure. The pore distribution also appears to be random in the structure and this could be basis for low BET surface area and low pore volume reported earlier.

The FTIR analysis showed that wood biochar had very low intensity bands in regions of 3600–3000, 2920–2800 and 1000–400 cm^{-1}. The intensity of 3600–3000 cm^{-1} could be attributed to stretching of hydroxyl (O-H) functional groups due to dehydration of the holocellulose. The observed peaks in the 2920 cm^{-1} and 2850 cm^{-1} could be attributed to aliphatic methyl and methylene groups while the peaks between 1000 and 400 cm^{-1} indicated C–H stretching within the aromatic rings. The absence of bands in the range of 2000–1000 cm^{-1} indicated great aromaticity and/or suggests that the wood residues underwent complete pyrolysis during the charring process with loss of oxygen-containing species. Rice husk biochar on the other hand exhibited more surface complexity with several peaks. The most predominant peak was in the range of 3399 cm^{-1} and corresponded to the stretching of OH groups preferably from aliphatic alcohols and phenols. The peak at 1599.12 cm^{-1} indicated high aromaticity and corresponded to presence of alkyl and alkene groups (C–H, C═C and C–C) from the stretch of aromatic rings. The peaks between 1099 and 798.79 cm^{-1} may be due to the stretching of silicon containing groups (Si–O–Si) given that rice usually has large amounts of silicon, while the peak of 467 cm^{-1} can be attributed to C–H stretching in the aromatic rings. This interpretation of FT-IR results is based on previous biochar studies by (Abdulrazzaq et al., 2014; Fu et al., 2012; Keiluweit et al., 2010; Kim et al., 2013; Mukherjee et al., 2011).

3.2. Amount of NH_4^+-N adsorbed

The maximum adsorbed amount from pure solution and digestate slurry by wood biochar was 54.84 $mg \cdot g^{-1}$ (73%) and 44.64 $mg \cdot g^{-1}$ (60%), respectively. The maximum adsorbed amount by rice husk biochar was 44.64 $mg \cdot g^{-1}$ (60%) and 39.8 $mg \cdot g^{-1}$ (53%) for NH_4Cl and slurry respectively. As hypothesized earlier the adsorption from pure

Table 6
Thermodynamic parameters for NH_4^+-N sorption from slurry and pure solutions onto biochar at 1000 mg/L.

Temp. (K)	K_c	ΔG^o ($kJ \cdot mol^{-1}$)	ΔH^o ($kJ \cdot mol^{-1}$)	ΔS^o ($J \cdot mol\ K^{-1}$)	R^2
Rice husk biochar					
288.15	0.91 (0.91)	0.214 (0. 215)	17.13 (17.661)	−172.4 (−174.8)	0.984 (0.912)
298.15	1.25 (1.66)	−0.547 (−1.257)			
308.15	1.53 (3.46)	−1.086 (−3.185)			
318.15	1.91 (3.20)	−1.715 (−3.077)			
Wood biochar					
288.15	1.03 (1.53)	−0.078 (−1.021)	35.05 (38.83)	−350.85 (−377.04)	0.987 (0.977)
298.15	1.42 (2.74)	−0.868 (−2.502)			
308.15	1.72 (5.00)	−1.385 (−4.126)			

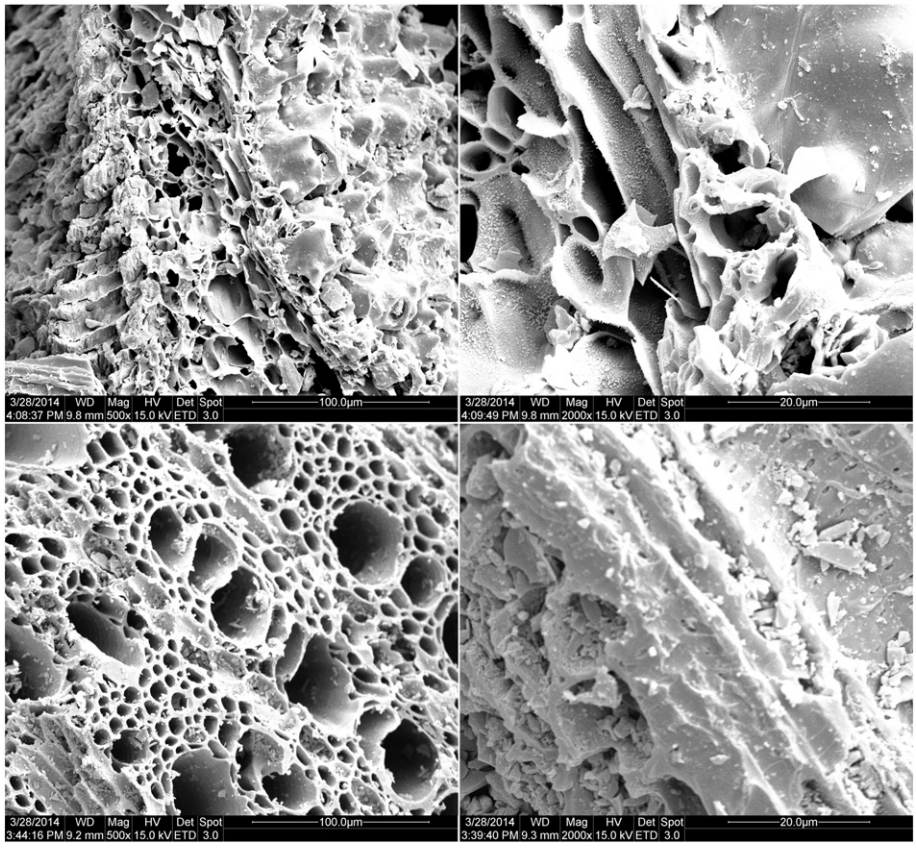

Fig. 1. Scanning electron microscopy images of rice husk biochar at magnification × 500 (top left) and × 2000 (top right), and wood biochar at magnification × 500 (bottom left) and × 2000 (bottom right).

solution was higher than adsorption from digestate slurry. Similarly, the removal percentage and adsorbed amount in both pure solution and slurry was significantly higher with wood biochar than rice biochar (Table 7). The higher adsorption with wood biochar could be due to its superior BET surface area (Table 1). Regarding adsorption from slurry, our results contradict those reported by Sarkhot et al. (2013) who studied ammonium sorption from diary slurry using mixed wood residues biochar. In their study, the authors observed a two-fold increase in NH_4^+ from slurry than in pure solution and concluded that the presence of dissolved matter in the slurry could have fostered an increase in adsorption. We argue our case for the lower adsorption from digestate slurry by linking it to the presence of competing ions. As shown in Table 2, the sample pretreated slurry contained a reasonable amount of cations in the order K > Na > Ca > Mg > Fe and Zn and we highly anticipate that through competition with NH_4^+ for the adsorbent active sites, these ions were responsible for the decreased NH_4^+ adsorption from the slurry.

Table 7
One Way ANOVA depicting differences in NH_4^+ adsorbed (Q_e, $mg \cdot g^{-1}$) by biochar at initial conc. (1000 $mg \cdot L^{-1}$) pH = 7, temperature (303 K) and particle size (0.25 mm) from pure NH_4Cl solution and Pretreated Slurry.

Group	N	Mean	Std Dev	SEM	
WDB_1	4	39.609	3.105	1.174	
WDB_2	4	31.552	2.621	0.991	
RHB_1	4	34.426	3.125	1.181	
RHB_2	4	30.549	1.658	0.627	
Source of Variation	**DF**	**SS**	**MS**	**F**	**P**
Between groups	4	4747.940	1186.985	176.136	<0.001
Residual	11	202.170	6.739		
Total	15		34	4950.110	
Comparison[a]	**Diff of means**	**LSD (α = 0.05)**	***P***	**Diff > = LSD**	
WDB_1 vs. WDB_2	8.057	2.834	<0.001	Yes	
WDB_1 vs. RHB_1	5.183	2.834	<0.001	Yes	
RHB_1 vs. RHB_2	3.878	2.834	0.009	Yes	
WDB_2 vs. RHB_2	1.003	2.834	0.475	No	

1 and 2 denote adsorption from pure NH_4Cl solution and pretreated slurry respectively.
[a] All pair wise multiple comparison procedure (Fisher LSD method).

3.2.1. Effect of biochar dosage on amount of NH_4^+-N adsorbed

The results (Fig. 2a) indicated that increasing the mass of the biochar from 0.1 to 1.5 g increased the percentage of NH_4^+ removal and equilibrium adsorbed amount onto biochar. However, for biochar > 1 g, the removal efficiency and adsorbed amount ($mg \cdot g^{-1}$) gradually decreased. The increase in both removal percentage and adsorbed amount ($mg \cdot g^{-1}$) with biochar dosage could be attributed to the increased number of available adsorption sites as the solid mass increases in solution. Conversely, the gradual reduction beyond 1 g could be due to the overlap of absorbent layers a phenomenon that shields available active sites on the absorbent as the mass of the solids increases. Similar adsorption studies using biochar and different absorbents for NH_4^+ have reported the same effect e.g., with ion exchange resin (Sica et al., 2014), with zeolites (Huang et al., 2010; Saltali et al., 2007) and with activated carbon (Long et al., 2008).

3.2.2. Effect of increasing NH_4^+ concentration in solution on amount of NH_4^+-N adsorbed

The results (Table 3) and (Fig. 2c) indicate that when the initial concentration was low i.e., between 250 and 500 $mg \cdot L^{-1}$, the NH_4^+ removal efficiencies from the wastewater were higher and they were 80.4 to 89% for NH_4Cl and 76 to 80% from the slurry for wood and rice husk biochar

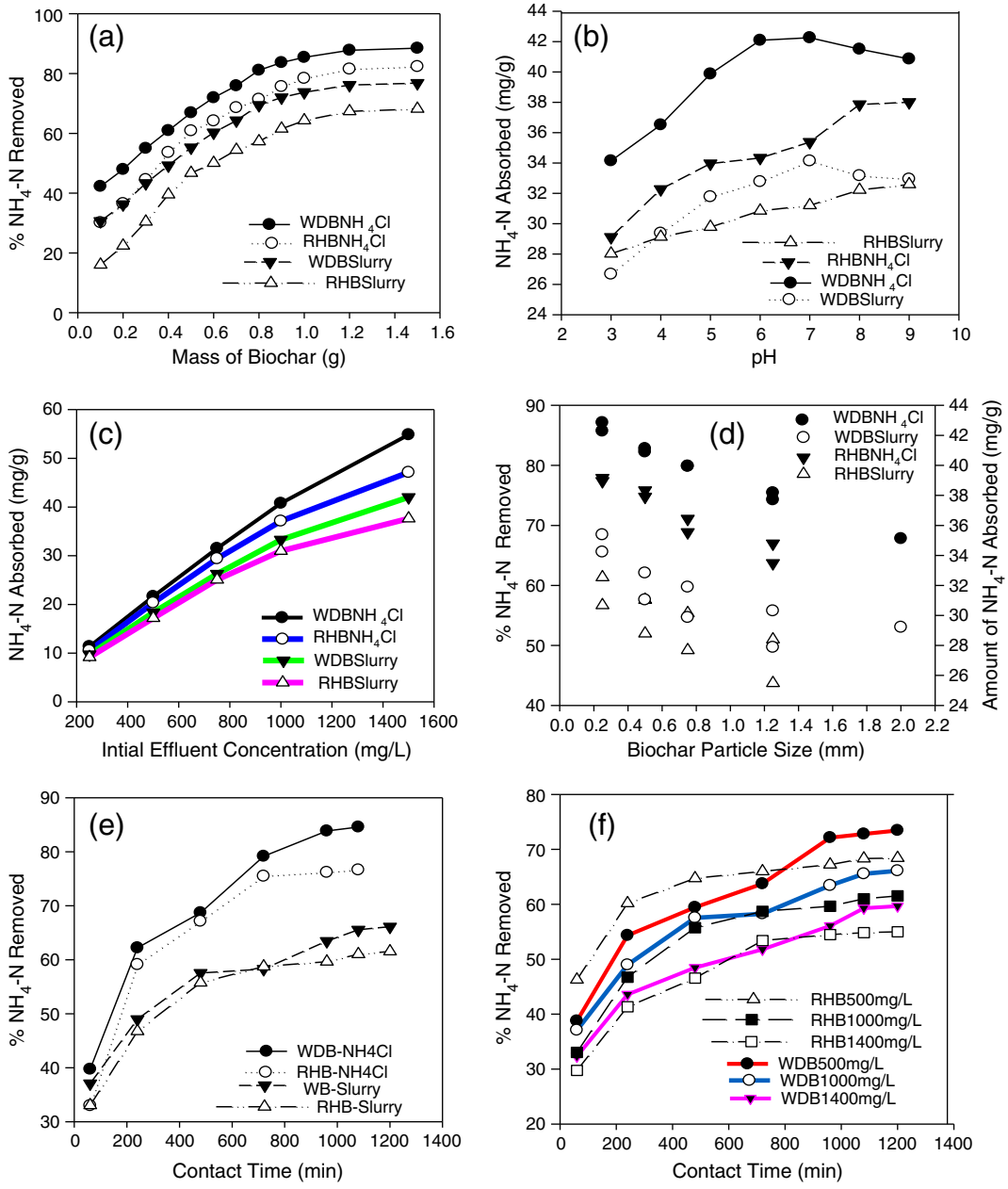

Fig. 2. Effect of biochar mass (a), pH (b), initial NH_4^+-N concentration (c), particle size (d), contact time (e) and time effect at different slurry concentrations (f) on NH_4^+ adsorption.

respectively. As the concentration increased from 750 to 1400 mg·L^{-1} the removal efficiency deceased but, the amount adsorbed (mg·g^{-1}) at equilibrium (Q_e) increased significantly. The implication of this could be that at low concentration there is equally low mass flow of ions and thus there are excess unoccupied active sites on the biochar and therefore the adsorption becomes dependent on the initial concentration (Nidheesh et al., 2012; Qu et al., 2008). However, as the concentration of ions increases there is correspondingly an increased mass flow of NH_4^+ to the biochar active sites due to the build-up of an ionic gradient between the solid and liquid phase and hence an increased adsorbed amount (Hema and Arivoli, 2007). Some studies have also suggested that at higher concentrations the ionic mobility becomes less random and the kinetics then follows electrostatic attraction between the absorbent and absorbate (Long et al., 2008).

3.2.3. Effect of pH on amount of NH_4^+-N adsorbed

Fig. (2b) shows the effect of initial solution pH on the adsorption of NH_4^+ at 1000 mgN·L^{-1} nutrient concentration. From the figure, at low pH of 3 to 4 both the percentage removal and amount adsorbed are lower, however, as the pH increases from 4 to 8 both the percentage removal and amount adsorbed (mg·g^{-1}) increase. At pH > 8, the adsorption takes a decreasing trend. The decrease in adsorption at pH > 8 could be attributed to the fact that most of the NH_4^+ is converted to NH_3 which cannot be adsorbed onto the adsorbent (Huang et al., 2010). On the other hand, the decreased NH_4^+ removal at lower pH could due to the high protonation of functional groups (C═O, COO^-) on the biochar surfaces which impart a partial positive charge that repels the polar attraction of NH_4^+ ions in aqueous solution (Novak et al., 2010). Some previous ammonium sorption studies using zeolites and activated carbon have reported similar results (Halim et al., 2013; Kucic et al., 2013; Thornton et al., 2007).

3.2.4. Effect of particle size on amount of NH_4^+-N adsorbed

The effect of particle size on the NH_4^+ adsorption is reported in Fig. 2d. From the figure it can be observed that adsorption efficiency for both biochars decreased with increasing the particle size. For wood biochar, the

percentage removal decreased from 69% to 53% while for rice husk biochar it decreased from 61 to 51% as the particle size increased from 0.25 to 1.25 mm. This trend can be linked to the relationship between the surface area of the adsorbent and rate of diffusion of the absorbate. Conventionally, surface area increases with smaller particle sizes and assuming that the rate of sorption is solely dependent on the surface area, then smaller adsorbent particles would have shortened diffusion paths because they present a better opportunity for absorbate ions to penetrate all internal pore structures (Demirbas, 2004; Saltali et al., 2007). And this explains high absorption at low particle size. From kinetic experiments however, we found that although the uptake was higher with smaller particle sizes (0.25–0.5 mm) the equilibrium time was not significantly different and this could be that diffusion was not the sole limiting factor. Our results corroborate with previous studies (Huang et al., 2010; Wen et al., 2006) who investigated NH_4^+-N adsorption using zeolites and all reported a decrease in removal and adsorption with increased particle size.

3.2.5. Effect of contact time on amount of NH_4^+-N adsorbed

The effect of contact time was investigated for a period of 24 h using an initial NH_4^+-N concentration of 1000 $mg \cdot L^{-1}$ at 35 °C and pH = 7.0. The results (Fig. 2e and f) show that the NH_4^+ adsorption increased with time much more linearly for the first 6–8 h and then it plateaus. Furthermore, in 6 to 8 h, half of the total removed and adsorbed amount of on amount of NH_4^+-N occurred from both pure NH_4Cl and slurry after that the adsorption gradually becomes slower until equilibration. The trend could be explained in three ways; first the initial rapid uptake is a physical process occurring mainly through mass transfer based on ion concentration gradient between the solid and liquid phases (Halim et al., 2013; Long et al., 2008; Zhu et al., 2012). The second slower phase depicts the end of physical sorption and corresponds to the ionic balance between the solid and liquid phase with slight desorption occurring for the physically bound NH_4^+ ions. Finally, the much slower and more gradual increment corresponds to chemisorption and some extent intrapartical diffusion which continues until saturation of the active sites (Kucic et al., 2013; Qu et al., 2008). A similar trend has been reported in other studies (Saltali et al., 2007; Wen et al., 2006) however, their equilibration time is much shorter than what we report probably because the concentrations they studied are much lower than ours and adsorption was based on zeolites.

3.2.6. Effect of temperature on amount of NH_4^+-N adsorbed

An initial NH_4^+-N concentration of 1000 $mg \cdot L^{-1}$ adsorption was investigated at different temperatures i.e., 15, 20, 25, 30, 35, 40, 45 °C. The results (Fig. 3) showed that adsorption increased with temperature. However, there was a sharp contrast between adsorption in the pure NH_4Cl solution and slurry. For the slurry, the amount adsorbed increased with temperature more linearly up to 45 °C whereas for pure solution the maximum adsorption for both rice husk and wood biochar was achieved at much lower temperature (30 °C). The finding suggests that NH_4^+ adsorption from the slurry is more endothermic and thus temperature above the ambient will be required in order to achieve maximum adsorption. The trend can be explained using the ideas presented by Long et al. (2008) and Zhu et al. (2012) who suggested that at higher temperatures the diffusivity of absorbate (NH_4^+) from the external laminar layer into the micro pores of the biochar increases due to the higher reaction rate between the NH_4^+ and biochar surface functional groups.

3.3. Sorption isotherms

Table 4 shows the values of maximum adsorption capacities (α and β), the rate constants K_L, K_F, $1/n$ and the regression coefficients (R_L^2 and R_F^2) for the Langmuir and Freundlich models, respectively. The individual isotherms are presented in Fig. 4. From Table 4, the values of R_L^2 for wood and rice biochar were 0.995 and 0.993 for the slurry, and were higher than the corresponding Freundlich R_F^2 values (0.987 and 0.977). Therefore, on the basis of the observed R^2 values the Langmuir model fitted the data better suggesting that NH_4^+-N adsorption much occurred by chemisorption within the monolayer. On the other hand, although the R_F^2 values from the Freundlich model were all >0.95 suggesting some level of physical adsorption, the values of $1/n > 1$, implied chemisorption was slightly more favorable. Similar biochar adsorption studies have reported NH_4^+-N adsorption to fit both the Langmuir and Freundlich models (Liu et al., 2010, 2013; Zhu et al., 2012). In these studies the result has been greatly attributed to the heterogeneous nature of biochar surfaces.

3.4. Sorption kinetics

The best model fits for the pseudo first and second order kinetics were selected based on both regression coefficient (R^2) and the calculated q_e values. The calculated q_e ($mg \cdot g^{-1}$) was compared to the experimental value (Q, $mg \cdot g^{-1}$) and a judgment was made; that if the calculated q_e was close in range to the experimental (Q) value, then data fitted well. Another consideration was based on the regression coefficient (R^2), if it was ≥0.95 then the model fitted the data. Conversely, for the intrapartical model, interpretation was made based on the K_d value, intercept value (C) and R^2 values. The model was only considered to fit the data if the plot of Q_t verses $t^{1/2}$ was linear passing through the origin and if R^2 was > 0.95. Table 5 shows the calculated values of (Q_1, Q_2, C), the rate constants (λ_1, λ_2, K_d) and R^2 values for the pseudo first and second order kinetic and intrapartical models, respectively. The isotherm curves for the individual models are presented in Fig. 5. From Table 5 above, several deductions were made. Firstly, the earlier assumption by the intrapartical model that during NH_4^+ adsorption onto the biochar, the inner particle diffusion is the major adsorption mechanism was rejected. This conclusion was reached based on the R^2 values which were <0.95. In addition, the large values of the intercept

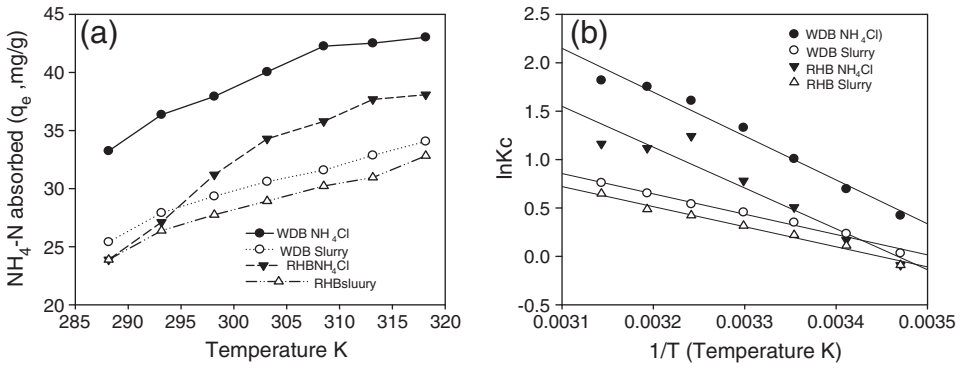

Fig. 3. (a) effect of temperature on NH_4^+ sorption and (b) vant Hoff's model explaining the process thermodynamics of NH_4^+-N onto biochar.

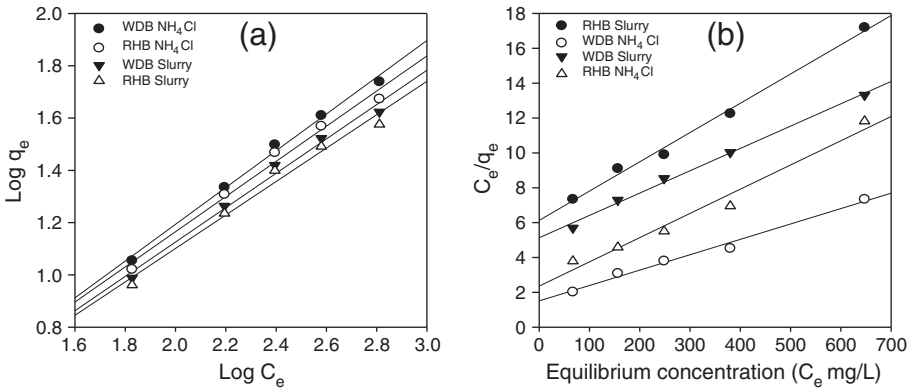

Fig. 4. (a) Freundlich adsorption model and (b) Langmuir adsorption model.

clearly indicate that the line plots of q_t vs. $t^{1/2}$ are far from the origin, confirming that the intrapartical diffusion couldn't be a rate limiting factor, thus other forces were in counter play (Halim et al., 2013; Liu et al., 2010).

Secondly, it was noticed that the values of the correlation coefficients (R^2) for the pseudo-second order model are higher than those for pseudo-first-order model for both biochars and in both nutrient solutions implying the experimental data were better fitted by the pseudo-second order equation. Furthermore, comparing the calculated maximum adsorption values (Q_1 and Q_2) with the experimental values (q_e), the calculated values (Q_1) for the pseudo-first-order model were lower than the experimental values whereas the calculated values from the pseudo-second-order model (Q_2) were in close range or even higher than the experimental values further confirming a better data fit to the pseudo-second order kinetic model. Based on the better fit by the pseudo second order model it can be deduced that, some part of the adsorbed NH_4^+-N onto the biochar occurred by chemisorptions (Ho and McKay, 1999; Zhu et al., 2012).

Interestingly from Table 5, the intensity of NH_4^+ adsorption predicted in both the pseudo-first order and the second order models is higher with rice husk biochar. This finding supports the idea that NH_4^+ was not solely dependent on large surface area because if it were the case then wood biochar would have had higher adsorption intensity. Likewise, the high adsorption rate (v = 2.37 and 2.46) observed with rice biochar for both pure solution and slurry and the corresponding high R^2 values (0.999 and 0.995) suggest some kind of chemical interaction probably via covalent bonding between the rice husk biochar and NH_4^+ (Hema and Arivoli, 2007). These results can also be used to understand the closeness in adsorption between the wood and rice biochar based on the slurry (Table 3). In reality basing on the BET surface area one would expect wood biochar to show superior adsorption than rice biochar in both effluents. More so, from the FT-IR results (Section 3.1) rice biochar exhibited more surface complexity with a wider range of functional groups than wood biochar. It could be that the presence of these groups greatly enhanced NH_4^+-N adsorption by rice husk biochar in the slurry even if it had a low surface compared to wood biochar.

3.5. Sorption thermodynamics

Table 6 shows the values of K_c, ΔG^o, ΔH^o ΔS^o and the regression coefficients (R^2) at different sorption temperatures based on initial NH_4^+-N concentration of 1000 mg·L^{-1}. From Table 6, the values of $\boldsymbol{\Delta H^o}$ for wood biochar are 35.049 and 38.834 from slurry and NH_4Cl solution respectively. For the rice husk biochar, the values were 17.132 and 17.661 for slurry and NH_4Cl solution respectively. A graphical comparison between rice husk and wood biochar in NH_4Cl and slurry at different temperature is presented in Fig. 3b. Also from Table 6, it can be observed that K_c increased with temperature. This increase in K_c and the positive standard enthalpy change (ΔH^o) indicated that NH_4^+ adsorption process was endothermic. The negative Gibbs free energy (ΔG^o) values were in the range of 0 to 20 kj.mol^{-1} indicating that the process of NH_4^+ adsorption onto the biochar was mainly physical and spontaneous in nature (Qu et al., 2008; Wen et al., 2006). Likewise, the positive and higher ΔS values further suggest increased disorder and randomness of liquid–solid phase interaction at the biochar surface (Hema and Arivoli, 2007). It is important to note that although the equilibrium and kinetic data suggest chemisorption as the major mechanisms of NH_4^+ adsorption onto the biochar, the thermodynamic parameters point out

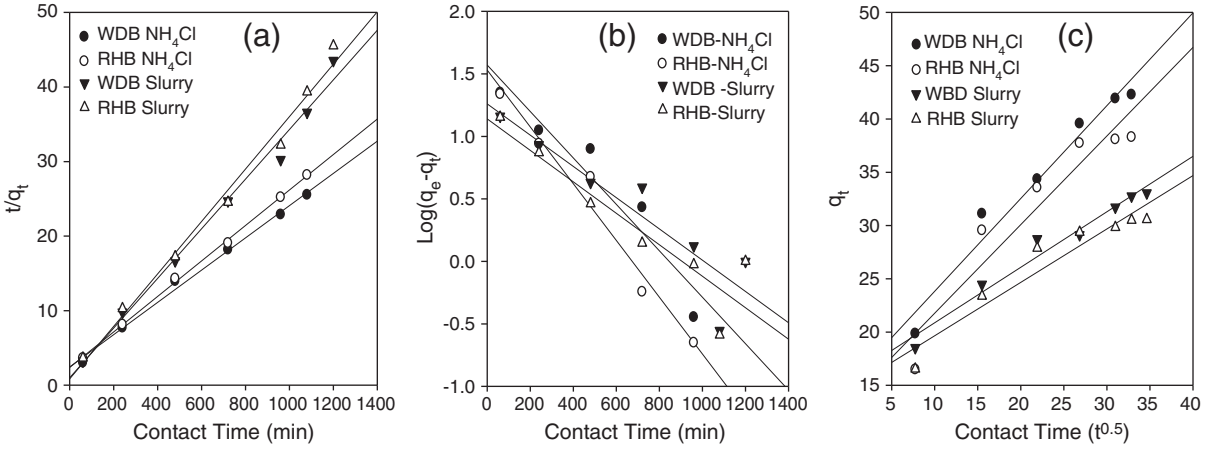

Fig. 5. Plots for the pseudo second order model (a), Pseudo first order model (b) and Intrapartical model (c).

occurrence of physical absorption. The conclusion can be made that both chemisorption and physical adsorption occur.

4. Conclusions

This study investigated the potential use of biochar for NH_4^+-N adsorption from piggery manure anaerobic digestate slurry. The results show that at low to medium range concentrations (250–1000 $mg \cdot L^{-1}$) both biochars performed well by adsorbing 70–80% while at higher loading 1000–1400 $mg \cdot L^{-1}$ up to 50% of the NH_4^+ was adsorbed. The maximum adsorption was sensitive to temperature, particle size and pH. The most favorable particle size that in range of >0.25 to 0.5 mm while maximum absorption was observed to occur at pH 6.5–7.0 and significantly decreased at low pH (3–4) and very highly alkaline pH >8. In addition, the adsorption process was endothermic, implying that in practice there is a need to raise the temperatures above 30 °C to a maximum of 45 °C. The results also point out the fact that the presence of heavy metals in slurry greatly interferes with the NH_4^+ adsorption and thus needs to be reduced to achieve reasonable adsorption. Chemisorption involving ionic bond formation with surface functional groups and surface area dependent physical diffusion were the most likely mechanisms of NH_4^+ adsorption. Overall results suggest wood and rice husk biochar can be successfully used for ammonium removal from piggery slurry on a broad concentration range.

Conflict of interest

There is absolutely no conflict of interest be it financial or relational during the preparation and submission of this work.

Acknowledgement

This work was financed by grants from the project of “The National Natural Science Funds (51308536)”, “Specialized Research Fund for the Doctoral Program of Higher Education (20130008120018)” and “Fund for supervisor of excellent PhD dissertation of Beijing City (20131001903)”. We likewise greatly appreciate the critical and constructive comments from the anonymous reviewers, which have helped improve this manuscript.

References

Abdulrazzaq H, Hamdan J, Ahmed H, Abu-Bakr R. Characterization and stabilisation of biochars obtained from empty fruit bunch, wood, and rice husk. Bioresources 2014; 9(2):2888–98.
Ahamedna M, Marshall WE, Rao RM. Production of granular activated carbons from selected agricultural by-products and evaluation of their physical, chemical and adsorptive properties. Bioresour Technol 2000;71(2000):113–23.
Ahmedna M, Johns MM, Clarke SJ, Marshall WE, Rao RM. Potential of agricultural by-product-based activated carbons for use in raw sugar decolorization. J Sci Food Agric 1997;75:117–24.
Al-Wabel MI, Al-Omran A, El-Naggar AH, Nadeem M, Usman AR. Pyrolysis temperature induced changes in characteristics and chemical composition of biochar produced from conocarpus wastes. Bioresour Technol 2013;131:374–9.
Amuda OS, Giwa AA, Bello IA. Removal of heavy metal from industrial wastewater using modified activated coconut shell carbon. Biochem Eng J 2007;36(2):174–81.
APHA. Standard methods for the examination of water and wastewater. 20th ed. New York, USA: American Public Health Assiociation; 2005.
ASTM. ASTM D1762 84: standard test method for chemical analysis of wood charcoal. ASTM International; 2007. p. 2 [D 1762-84(2007)].
Chen RJ. Livestock–biogas–fruit systems in South China. Ecol Eng 1997;8:19–29.
Chen BL, Chen ZM, Lv SF. A novel magnetic biochar efficiently sorbs organic pollutants and phosphate. Bioresour Technol 2011;102(716–723):716.
Chen L, Zhao LX, Ren CS, Wang F. The process and prospects of rural biogas production in China. Energy Policy 2012;51:58–63.
China Ministry of Environmental Protection, S.S.B.a.M.o.A. First national census on pollution sources. China Government Press; 2010. p. 200 [February 9, 2010].
Değermenci N, Ata ON, Yildız E. Ammonia removal by air stripping in a semi-batch jet loop reactor. J Ind Eng Chem 2012;18(1):399–404.
Demirbas A. Effects of temperature and particle size on bio-char yield from pyrolysis of agricultural residues. J Anal Appl Pyrolysis 2004;72(2004):243–8.
FAO. Livestock's long shadow — environmental issues and options. Rome: FAO; 2006. p. 377.
Fu P, Hu S, Xiang J, Sun L, Su S, Wang J. Evaluation of the porous structure development of chars from pyrolysis of rice straw: effects of pyrolysis temperature and heating rate. J Anal Appl Pyrolysis 2012;98:177–83.
Gale F, Marti D, Hu D. China's volatile pork industry. Economic research service report. United States Department of Agriculture; 2012. p. 1–27 [LDP-M-211-01(2012)].
Ganrot Z, Dave G, Nilsson E. Recovery of N and P from human urine by freezing, struvite precipitation and adsorption to zeolite and active carbon. Bioresour Technol 2007; 98(16):3112–21.
Hale SE, Alling V, Martinsen V, Mulder J, Breedveld GD, Cornelissen G. The sorption and desorption of phosphate-P, ammonium-N and nitrate-N in cacao shell and corn cob biochars. Chemosphere 2013;91(11):1612–9.
Halim AA, Latif MT, Ithnin A. Ammonia removal from aqueous solution using organic acid modified activated carbon. World Appl Sci J 2013;24(1):01–6.
Harrington C, Scholz M. Assessment of pre-digested piggery wastewater treatment operations with surface flow integrated constructed wetland systems. Bioresour Technol 2010;101(18):6950–60.
Healy MG, Rodgers M, Mulqueen J. Treatment of dairy wastewater using constructed wetlands and intermittent sand filters. Bioresour Technol 2007;98(12):2268–81.
Hema M, Arivoli S. Comparative study on the adsorption kinetics and thermodynamics of dyes onto acid activated low cost carbon. Int J Phys Sci 2007;2(1):010–7.
Ho YS, McKay G. Pseudo-second order model for sorption processes. Process Biochem 1999;34(1999):451–65.
Huaitalla MR, Gallmann E, Liu XJ, Hartung E. Aerial pollutants on a pig farm in peri-urban Beijing, China. Int J Agric Biol Eng 2013;6(1):36–47.
Huang H, Xiao X, Yan B, Yang L. Ammonium removal from aqueous solutions by using natural Chinese (Chende) zeolite as adsorbent. J Hazard Mater 2010;175(1–3):247–52.
Keiluweit M, Nico Peter S, Johnson Mark G, Kleber M. Dynamic molecular structure of plant biomass-derived black carbon (biochar). Environ Sci Technol 2010;44(2010): 1247–53.
Kim WK, Shim T, Kim YS, Hyun S, Ryu C, Park YK, et al. Characterization of cadmium removal from aqueous solution by biochar produced from a giant Miscanthus at different pyrolytic temperatures. Bioresour Technol 2013;138:266–70.
Kucic D, Cosic I, Vukovic M, Briski F. Sorption kinetic studies of ammonium from aqueous solution on different inorganic and organic media. Acta Chim Slov 2013;60(2013): 109–19.
Liu H, Dong Y, Liu Y, Wang H. Screening of novel low-cost adsorbents from agricultural residues to remove ammonia nitrogen from aqueous solution. J Hazard Mater 2010;178(1–3):1132–6.
Liu N, Sun Z, Wu Z-C, Zhan X, Zhang K, Zhao E, et al. Adsorption characteristics of ammonium nitrogen by biochar from diverse origins in water. Adv Mater Res 2013; 664(2013):305–12.
Long XL, Cheng H, Xin ZL, Xiao WD, Li W, Yuan WK. Adsorption of ammonia on activated carbon from aqueous solutions. Environ Prog 2008;27(2):225–33.
Mizuta K, Matsumoto T, Hatate Y, Nishihara K, Nakanishi T. Removal of nitrate-nitrogen from drinking water using bamboo powder charcoal. Bioresour Technol 2004; 95(3):255–7.
Molle P, Prost-Boucle S, Lienard A. Potential for total nitrogen removal by combining vertical flow and horizontal flow constructed wetlands: A full-scale experiment study. Ecol Eng 2008;34(1):23–9.
Mukherjee A, Zimmerman AR. Organic carbon and nutrient release from a range of laboratory-produced biochars and biochar–soil mixtures. Geoderma 2013;193–194: 122–30.
Mukherjee AZ, A.R., Harris W. Surface chemistry variations among a series of laboratory-produced biochars. Geoderma 2011;163(3-4):247–55.
Mukherjee A, Lal R, Zimmerman AR. Effects of biochar and other amendments on the physical properties and greenhouse gas emissions of an artificially degraded soil. Sci Total Environ 2014;487(2014):26–36.
Nelson NO, Mikkelsen RL, Hesterberg DL. Struvite precipitation in anaerobic swine lagoon liquid: effect of pH and Mg:P ratio and determination of rate constant. Bioresour Technol 2003;89(3):229–36.
Nguyen ML, Tanner CC. Ammonium removal from wastewaters using natural NewZealand zeolites. N Z J Agric Res 1997;41:427–46.
Nidheesh PV, Gandhimathi R, Ramesh ST, Anantha Singh TS. Kinetic analysis of crystal violet adsorption on to bottom ash. Turk J Eng Environ Sci 2012;36(2012):249–62.
Nielsen A, Trolle D, Me W, Luo L, Han B-P, Liu Z, et al. Assessing ways to combat eutrophication in a Chinese drinking water reservoir using SWAT. Mar Freshw Res 2013; 64(5):475.
Novak JM, Busscher WJ, Watts DW, Laird DA, Ahmedna MA, Niandou MAS. Short-term CO2 mineralization after additions of biochar and switchgrass to a Typic Kandiudult. Geoderma 2010;154(3–4):281–8.
Qu B, Zhou J, Xiang X, Zheng C, Zhao H, Zhou X. Adsorption behavior of Azo Dye C. I. Acid Red 14 in aqueous solution on surface soils. J Environ Sci 2008;20(2008):704–9.
Rajkovich S, Enders A, Hanley K, Hyland C, Zimmerman AR, Lehmann J. Corn growth and nitrogen nutrition after additions of biochars with varying properties to a temperate soil. Biol Fertil Soils 2011;48(3):271–84.
Saltali K, Sari A, Aydin M. Removal of ammonium ion from aqueous solution by natural Turkish (Yildizeli) zeolite for environmental quality. J Hazard Mater 2007;141(1): 258–63.
Sarkhot DV, Ghezzehei TA, Berhe AA. Effectiveness of biochar for sorption of ammonium and phosphate from dairy effluent. J Environ Qual 2013;42(5):1545–54.
Sica M, Duta A, Teodosiu C, Draghici C. Thermodynamic and kinetic study on ammonium removal from a synthetic water solution using ion exchange resin. Clean Technol Environ Policy 2014;16(2):351–9.
Song YH, Qiu GL, Yuan P, Cui XY, Peng JF, Zeng P, et al. Nutrients removal and recovery from anaerobically digested swine wastewater by struvite crystallization without chemical additions. J Hazard Mater 2011;190(1–3):140–9.

Spokas KA, Novak JM, Venterea RT. Biochar's role as an alternative N-fertilizer: ammonia capture. Plant and Soil 2011;350(1–2):35–42.
Taghizadeh-Toosi A, Clough TJ, Sherlock RR, Condron LM. Biochar adsorbed ammonia is bioavailable. Plant and Soil 2012;350(1–2):57–69.
Thornton A, Pearce P, Parsons SA. Ammonium removal from digested sludge liquors using ion exchange. Water Res 2007;41(2):433–9.
Turker M, Celen I. Removal of ammonia as struvite from anaerobic digester effluents and recycling of magnesium and phosphate. Bioresour Technol 2007;98(8):1529–34.
Wen D, Ho YS, Tang X. Comparative sorption kinetic studies of ammonium onto zeolite. J Hazard Mater 2006;133(1–3):252–6.
Wrigley TJ, Webb KM, Venkitachalm H. A laboratory study of struvite precipitation after anaerobic digestion of piggery wastes. Bioresour Technol 1992;41(2):117–21.
Yang Y, Zhang P, Li G. Regional differentiation of biogas industrial development in China. Renew Sustain Energy Rev 2012;16(9):6686–93.
Zheng W, Guo M, Chow T, Bennett DN, Rajagopalan N. Sorption properties of greenwaste biochar for two triazine pesticides. J Hazard Mater 2010;181(1–3):121–6.
Zhu K, Fu H, Zhang J, Lv X, Tang J, Xu X. Studies on removal of NH_4^+-N from aqueous solution by using the activated carbons derived from rice husk. Biomass Bioenergy 2012;43:18–25.